

Offset-dependent mis-tie analysis at seismic line intersections

Daniel C. Huston* and Milo M. Backus‡

ABSTRACT

Offset-dependent line-intersection displays can be of significant direct interpretive value. On our data set from a proprietary location, use of these displays permits a refined structural interpretation and improves the usefulness of amplitude and amplitude-versus-offset displays for direct hydrocarbon detection. The degree of data reproducibility at each intersection may be exposed as a function of offset through the use of prestack and partial-range stack splice and difference displays.

At a set of marine line intersections, after only cursory processing, the range of residual amplitudes found by subtracting strike traces from dip traces is from -20 dB to +6 dB relative to the input. The average is about -8 dB. The poorest line intersection

ties occur below the edges of deep bright spots, where velocity anomalies leading to time mis-ties greater than 10 ms can occur. Shallow near-surface velocity anomalies, out-of-plane arrivals including fault plane reflections, and, occasionally, water reverberation variations contribute locally to the data mis-ties. Location errors are ubiquitous but of secondary importance, and random noise is more than 20 dB down.

A simple and inexpensive routine splice display of line intersection data can be of significant value for quality control, for processing evaluation, and for interpretation. Issues of data reliability, such as screening of amplitude-versus-offset (AVO) anomalies by shallow gas and transmission-path problems for large CMP offsets, as well as other problems in operational and research geophysics, may be addressed by analysis of line intersections in the offset domain.

INTRODUCTION

Seismic interpretation techniques have traditionally used the match in seismic response at line intersections as a check on accuracy. The hope is that processed seismic data show a reproducible subsurface target-zone response, invariant with line direction, at a line intersection. In this study, we examine the tie at a set of marine seismic line intersections and exploit differences in recorded responses to illuminate specific signal and noise effects. The analysis of line ties has been treated by White (1984) and Henry and Mellman (1988). Our work differs from previous line tie studies in that the offset dependence of the mis-ties is emphasized.

In a simple locally one-dimensional (1-D) earth, isotropic rock properties are a function of depth only. When this condition holds within the shot-receiver aperture, a given CMP experiment could be rotated through 360 degrees with no change in signal response. Except for ambient noise, the CMP gather data on a dip line and strike line would be

identical. In practice, the earth often exhibits significant lateral changes within the 2-4 km offset range in common use. Source-generated noise and primary signal transmission-path effects are then dependent on azimuth. To the extent that the offset-dependent response is azimuth independent, simple interpretation of normal moveout in terms of rms velocity and a simplified interpretation of amplitude and waveform variation with offset can be partially justified. Furthermore, inversion algorithms based on a locally 1-D earth model can be partially justified.

Since conventional processing is usually based on a locally 1-D earth model, an examination of offset-dependent mis-ties can provide an important processing quality control measure.

The data

Our data set (see Figure 1) is early 1970s vintage CMP seismic data from a shallow Tertiary clastic basin known as

Presented at the 56th Annual International Meeting, Society of Exploration Geophysicists. Manuscript received by the Editor August 3, 1988; revised manuscript received February 13, 1989.

*Unocal Science and Technology, P.O. Box 76, Brea, CA 92621-0076.

‡Department of Geological Sciences, Institute for Geophysics, University of Texas at Austin, P.O. Box 7909, Austin, TX 78713-7909.

© 1989 Society of Exploration Geophysicists. All rights reserved.

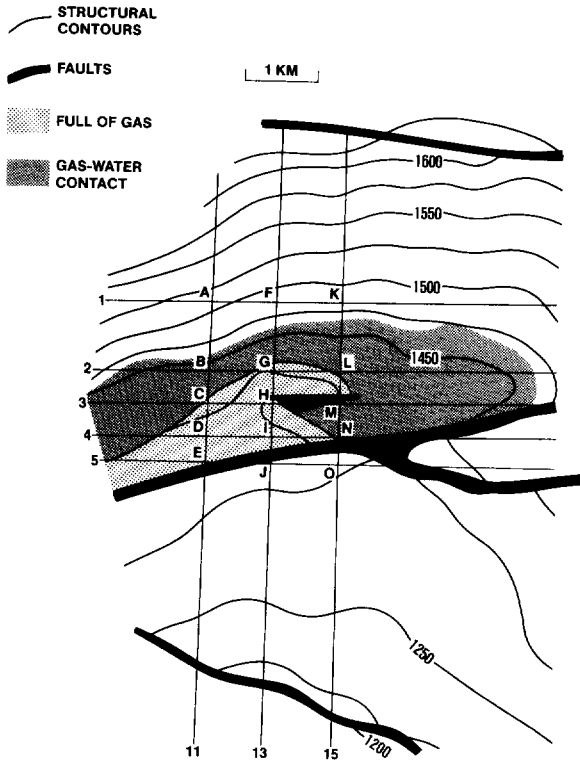


FIG. 1. Offshore Area One (OA1) base map (after Backus and Chen, 1975). Line intersections are marked by capital letters.

Offshore Area One or OA1 (Backus and Chen, 1975). The location is proprietary but it resembles offshore Nigeria. Large listric normal faults are present with apparent rollover into the fault on the down-thrown block. Figure 2 shows three dip lines for which we will examine 15 line intersections with the strike lines 1-5. No migration was applied so lateral resolution is not optimal. The zero-offset Fresnel zone is marked in line 15 at 1.7 s. Trace spacing is 50 m and maximum source-receiver offset is 2650 m. Figure 3 shows one intersecting strike line. In Figures 2 and 3, the large dots at the top indicate near-surface gas. Deeper commercial sized reservoirs of oil and gas have been penetrated in several wells. Event 4 marks a 40 m sandstone that appears to fill with gas updip; a clear gas-water contact reflection can be mapped at this level (Backus and Chen, 1975). Several other thinner reservoirs exhibit classical bright amplitudes when filled with gas. The five picked events were traced throughout the study area within the fault block to the left in Figure 2 and are annotated on the various displays in this paper.

PROCESSING METHODS

Moveout, scaling, and filtering

Normal moveout (NMO) and amplitude scaling for divergence corrections (Newman, 1973) were applied to all data on the basis of a simple, laterally invariant velocity function. The function is a quadratic fit of interpreted stacking velocity picks from the entire prospect:

$$V(t) = A + Bt + Ct^2, \tag{1}$$

where V = rms velocity in m/s at time t .

For OA1, rms velocities are 1.95 km/s at 1.0 s, 2.21 km/s at 1.5 s, and 2.45 km/s at 2.0 s. The same processing

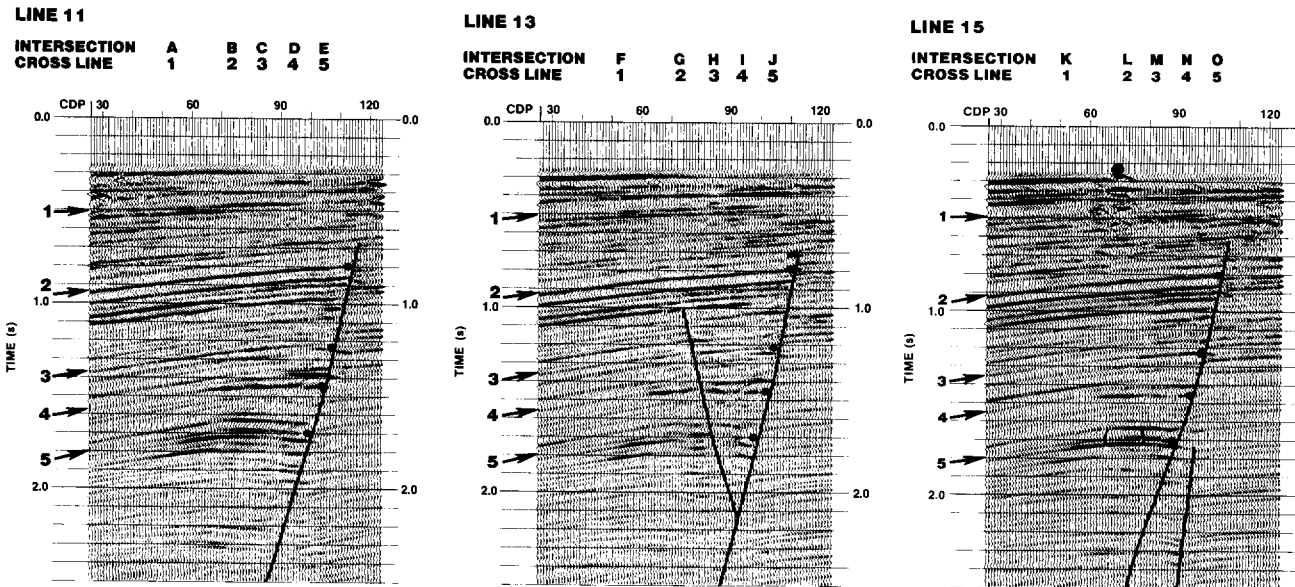


FIG. 2. Dip lines with line intersections marked at the top. Five events marked with arrows were interpreted in the block to the left of the major fault. Small dots indicate termination of events at the fault. On line 15, the large dot at the top indicates a shallow velocity anomaly and the zero-offset Fresnel zone is marked by parentheses at 1.7 s.

Table 1. Offset to depth ratio.

ODR 1 = minimum to 0.8	central angle = 18°
ODR 4 = 0.57 to 0.98	central angle = 26°
ODR 5 = 0.8 to 1.13	central angle = 32°
ODR 6 = 0.98 to 1.27	central angle = 38°
ODR 7 = 1.13 to 1.39	central angle = 42°
ODR 8 = 1.27 to 1.50	central angle = 46°
ODR 9 = minimum to 1.50	central angle = 25°

sequence was applied independently on all the lines, thereby eliminating changes in processing as a source of mis-tie.

Partial-range-stacks

The approach described by Todd and Backus (1985) was used to generate partial-offset-range stacks. On the basis of a specified velocity function (in this case the simple global function given above), time-variant offset ranges are calculated to correspond to particular offset-to-depth ratio (ODR) ranges. The ODR are selected such that the residual NMO range is the same within each partial-range stack. Furthermore, residual NMO increases linearly across a partial-range stacked CMP gather. This approach provides displays of

residual NMO moveout that can be interpreted readily. Table 1 shows how ODR correspond to specific local incidence angles. The angle refers to the central angle in the partial gather; there is a 50 percent overlap between adjacent gathers.

Line intersection displays

We expose mis-ties across offset with two types of gathers: difference records and splice displays. For general interpretation, we use a single display for each line intersection that shows dip- and strike-line CMP gathers interlaced. For a more quantitative assessment of the mis-tie, a difference record is produced by subtracting the strike-line CMP gather from the dip-line CMP gather at each line intersection.

The amount of residual energy remaining after subtraction provides a measurement of the degree of similarity between the two sets of seismic records through time and across offset and thus tests the assumption of lateral invariance within a CMP spread. The difference is very sensitive to arrival time mis-ties, and may be 6 dB stronger than the input traces for a half-period arrival time mis-tie. For a difference trace 10 dB down (about typical for this data set), the arrival

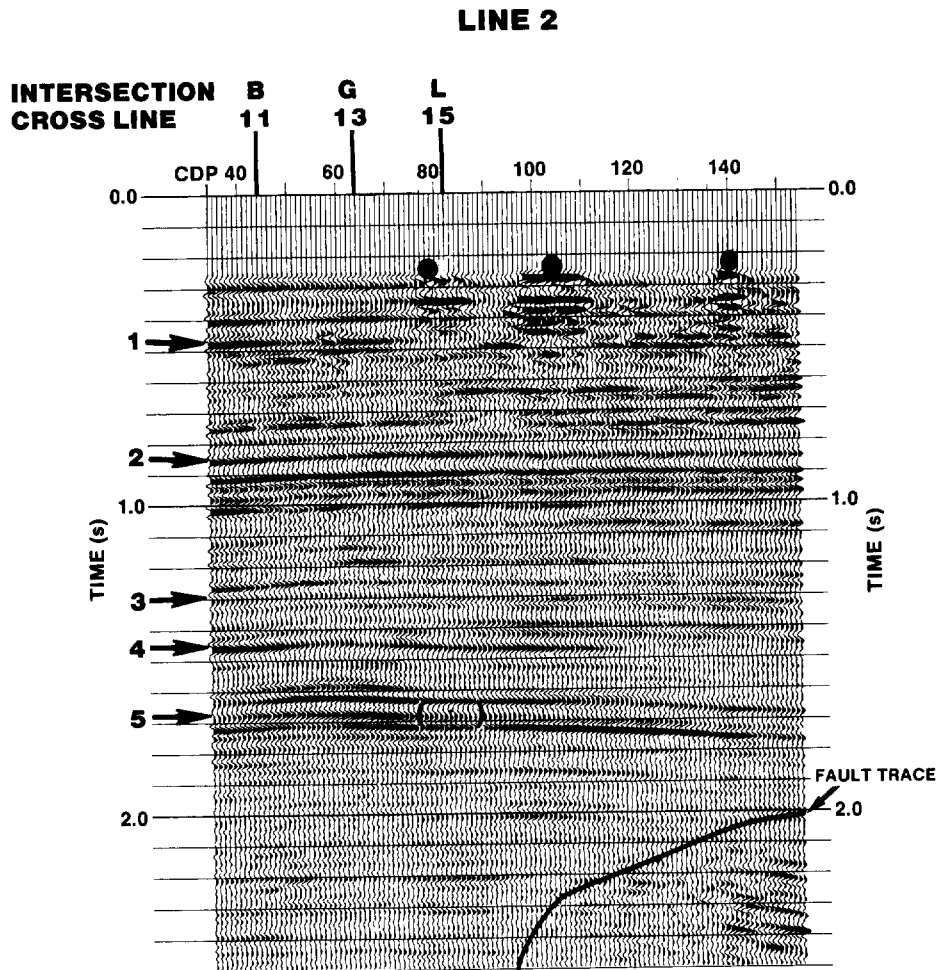


FIG. 3. Strike line 2 displayed in the same format as Figure 2. The fault trace indicates the major fault in Figure 2.

time mis-tie must be less than $1/20$ period, or 1.7 ms for 30 Hz data. A 30 percent amplitude mis-tie is thus comparable to a 1.7 ms time mis-tie in the difference trace approach. Processes aimed at forming a 1-D image can be evaluated by comparing their before and after performances in enhancing line ties with difference displays.

RESULTS

Prestack mis-ties

Most of the line intersections in our study area show no clear increase of mis-tie with increasing offset. Rather, on the difference records, certain offset and depth zones show relatively high residual amplitudes (+0 to +6 dB) against a low residual background (-6 dB to -10 dB). Figure 4 shows the CMP gathers at the crossing of dip line 15 with strike line 2 (intersection L). Only NMO and divergence correction have been applied to raw data. Strike-line intervals which appear poorly matched to the dip line are circled.

In Figure 5 another view of the match at intersection L is provided by splicing the two 48-fold gathers into a single

96-fold gather of dip-strike trace pairs. The diagonal lines indicate the ODR boundaries from 18 to 46 degrees local incidence angle. The localized nature of the mis-ties is more evident in this display format. The splice display highlights small time mis-ties, whereas amplitude mis-ties are more prominent in the Figure 4 format. Many OA1 line intersections show striking similarity in waveform character juxtaposed with relatively well defined mis-tied zones. For example, the farthest traces offset for event 4 are at approximately 50 degrees but tie very closely, while the same event is poorly tied at about 36 degrees local angle.

The CMP difference records before and after deconvolution are shown in Figure 6. No gain correction was applied, so amplitude with respect to trace spacing is the same as the input. Deconvolution is helpful across all offsets. However, as expected, deconvolution cannot completely eliminate the mis-tie. The residual after deconvolution is most pronounced in a zone of time and amplitude mis-tie at mid to far offsets on the difference section.

The stacked strike line (Figure 3) shows a near-surface bright spot near CMP 105 where Figure 6 shows a strong residual mis-tie. By ray tracing through a model based on our

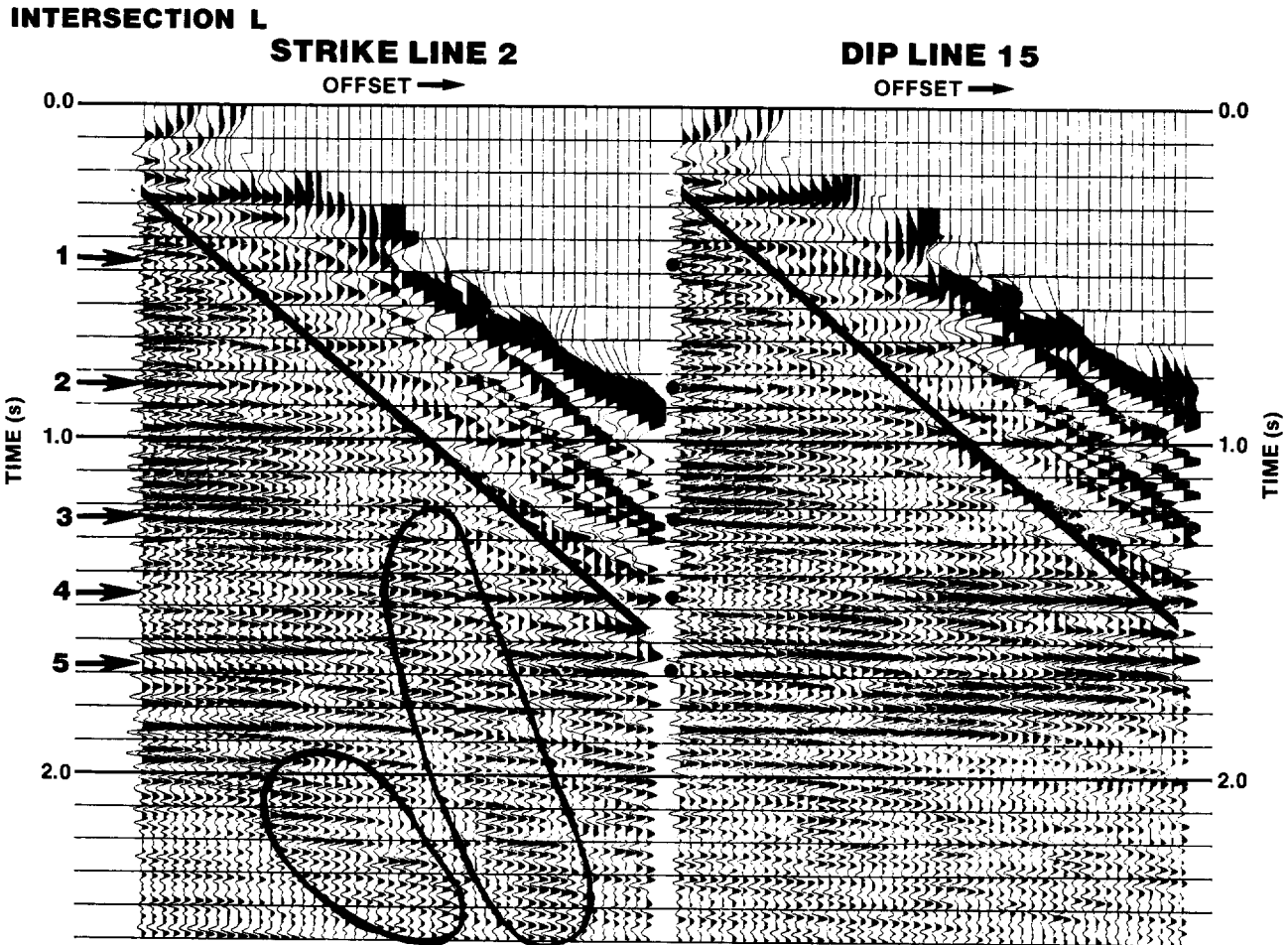


FIG. 4. CMP gathers located at the intersection of lines 15 and 2. NMO correction and divergence correction were applied but no deconvolution. The heavy diagonal line marks the mute zone boundary. Circled areas appear to be different on the dip-line gather.

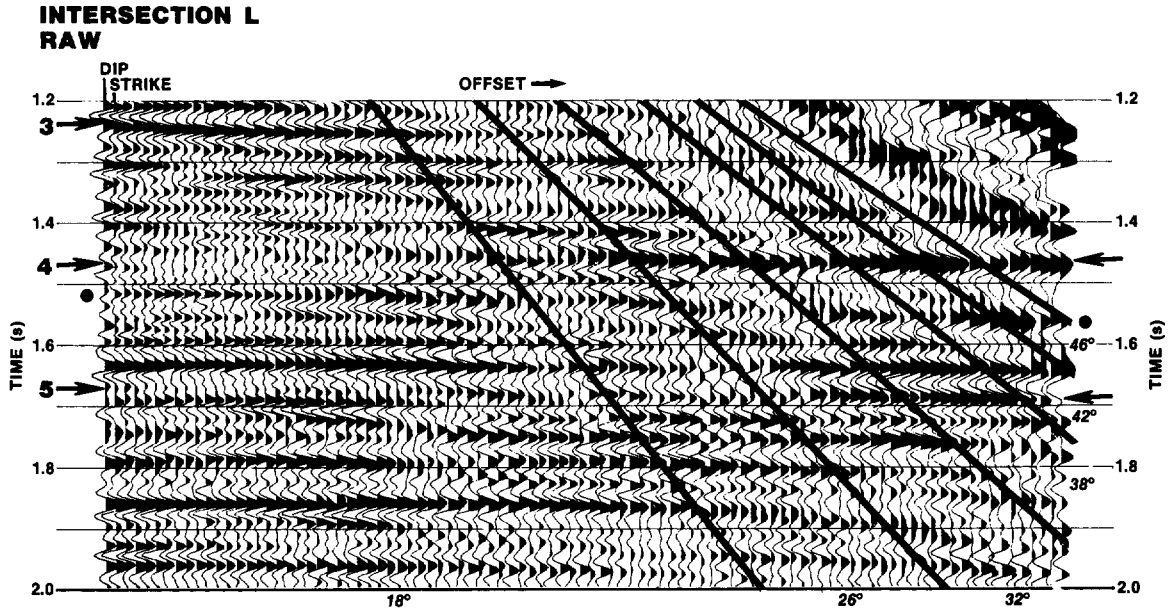


FIG. 5. Result of splicing the two intersecting 48-fold gathers from Figure 4 into a single 96-fold gather. Each pair of traces consists of a dip and then a strike trace at the same offset. No filtering was applied. Diagonal lines indicate the outer limits of the constant angle (ODR) ranges listed in Table 1. Arrows indicate primaries and the dots mark a reverberation at near and far offsets.

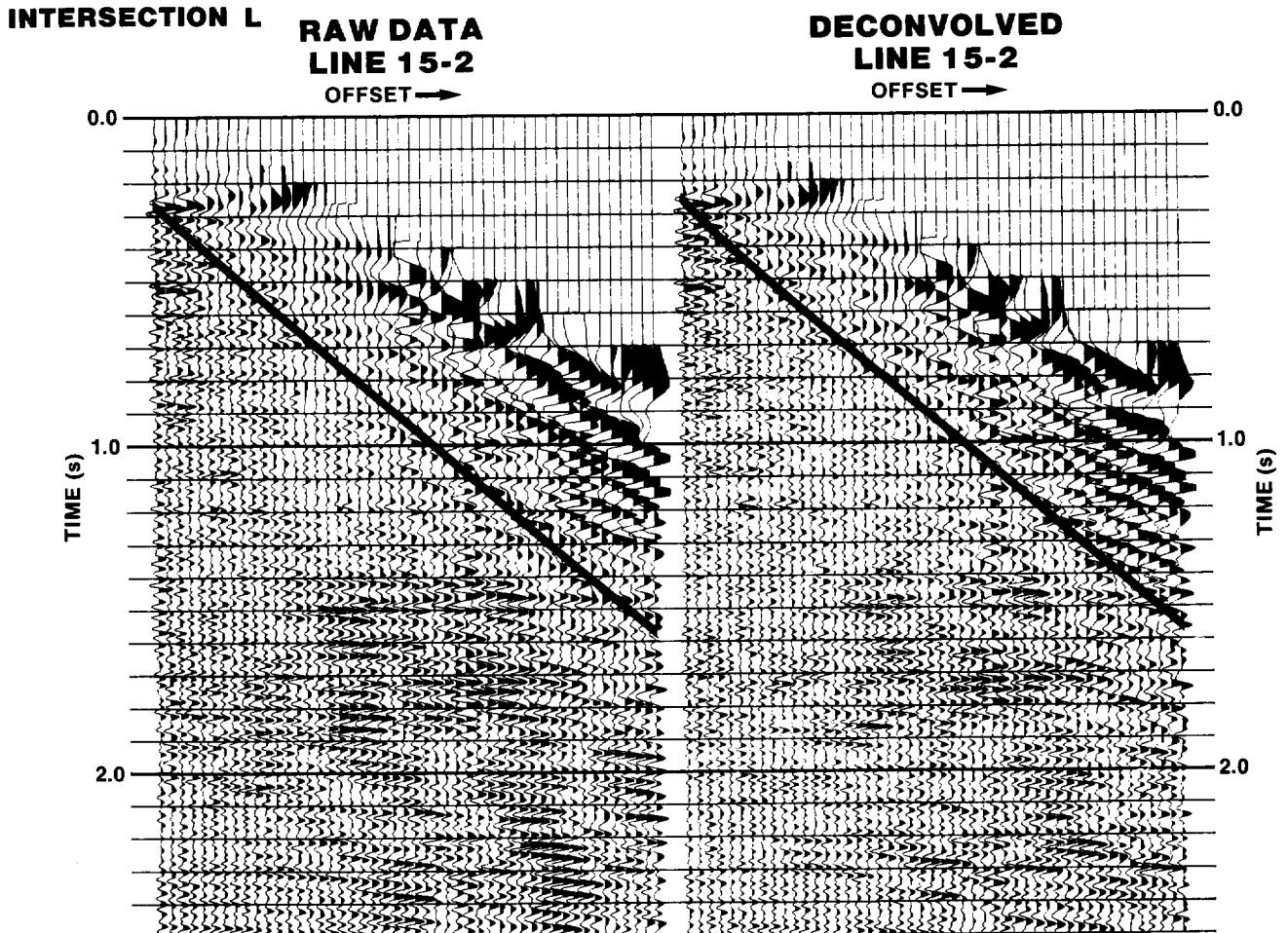


FIG. 6. Difference gathers formed by subtracting the strike line CMP traces from the dip line CMP traces in Figure 4. The deconvolved gather on the right was filtered with a 60 ms gap, 140 ms long operator prior to subtraction. The difference is not amplified with respect to the input.

global velocity function, travel paths through the near surface were related to times and offsets on the CMP gathers. Time delays and attenuation along travel paths through the shallow (gas) anomaly apparently account for most of the mis-tie remaining after deconvolution.

In cases where noise ties, the reduction of line-intersection mis-tie is an unreliable criterion for process evaluation. Although deconvolution enhances the prestack tie at intersection L, sometimes reverberations tie nearly as well as primaries. The expected moveout of water layer reverberations was calculated for various arrival times and compared to the observed moveout as a means of identifying multiples. At some locations in OA1, deconvolution did not greatly enhance the line tie, but periodic arrivals with the expected moveout were strongly attenuated.

The prestack data were analyzed rather extensively in an attempt to check and perhaps modify the source-receiver location data. No firm evidence of significant streamer feathering or location errors was found (Huston, 1987). Prestack data displays as in Figures 5 and 6 were also useful in quantifying the mis-ties for scattered energy and steeply dipping (e.g., fault plane) reflectors.

Partial stack data

The partial stacks corresponding to the spliced traces in Figure 5 are shown in Figure 7 along with a deconvolved version. Line intersection data that have been partially stacked and then spliced summarize offset-dependent ampli-

tude and waveform changes, along with providing information on the reliability of the seismic image across time and offset. Information about interval velocity is also provided and the signal-to-noise ratio is enhanced relative to that of the unstacked data. The mis-ties in arrival time and amplitude seen on the prestack data have been averaged across the corresponding partial stack ranges. Partial stacking alone can result in a substantial reduction in the apparent mis-tie. For example, event 4 on the spliced raw CMP gather is poorly resolved at near offsets with significant noise contamination and a relatively poor tie. After partial stacking, the arrival is weak but is resolved and ties quite well. Deconvolution changes the waveshape but not the tie.

A strong reverberation at about 1.52 s near-offset time is marked with dots at near and far offsets on the raw data in Figure 7. In this example, moveout is the main criterion for multiple identification. After deconvolution, the multiple has

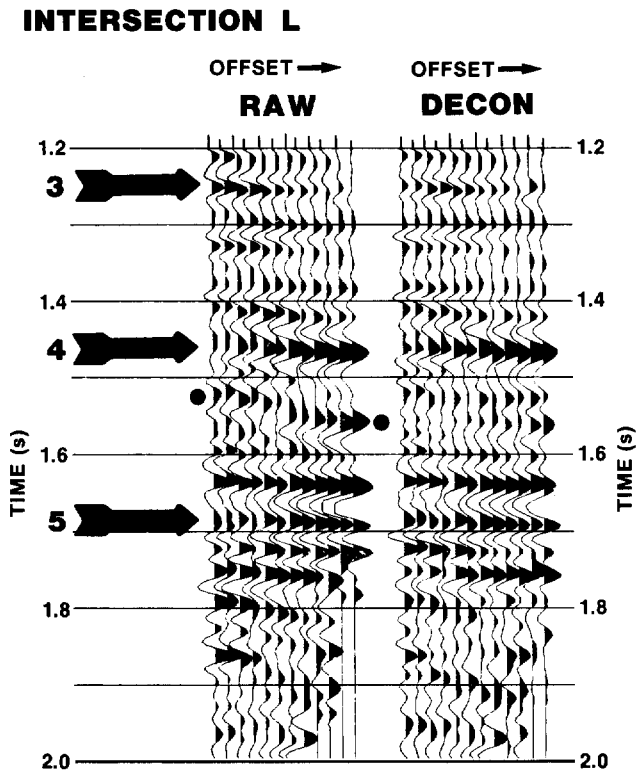


FIG. 7. Spliced partial stacks of the data in Figure 5 with and without gapped deconvolution applied after stack. Alternating dip and strike traces are plotted. The dots indicate a water-layer reverberation.

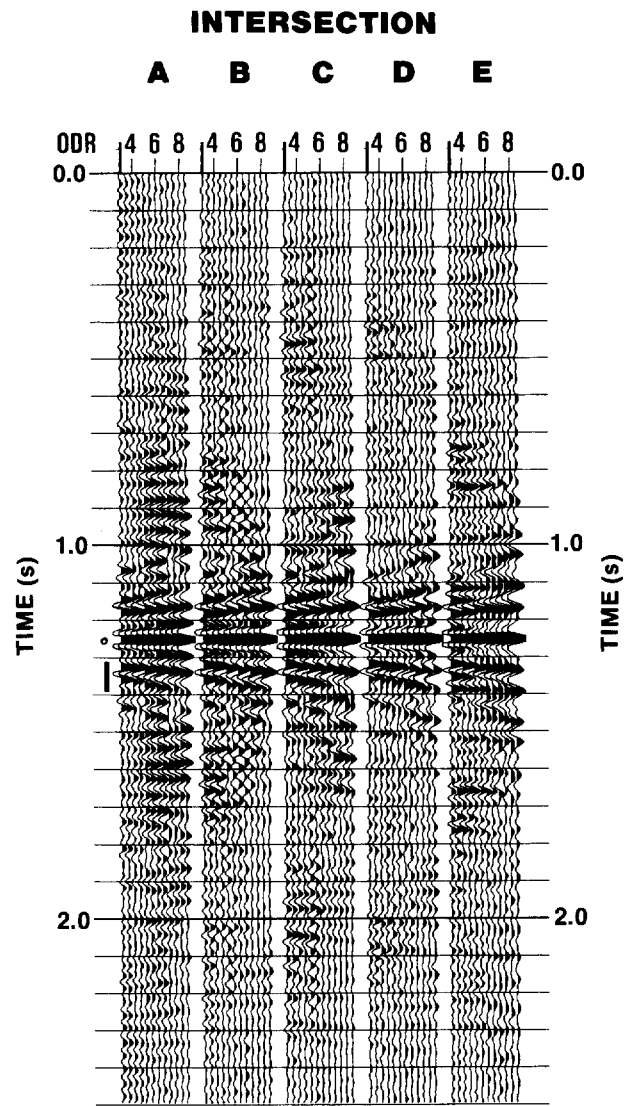


FIG. 8. Autocorrelograms formed from spliced partial stack traces at intersections on line 11. Zero lag is at 1.25 s. The active filter point range for the gapped deconvolution filter is indicated by the small vertical bar at the left.

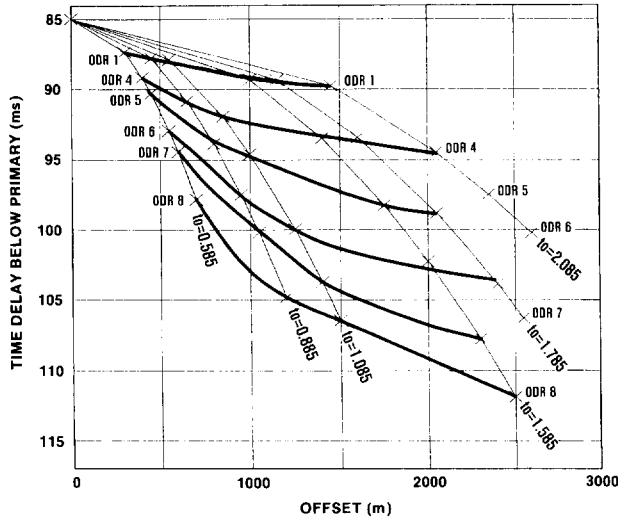


FIG. 9. Residual NMO curves for water-layer reverberations at selected times. Assuming accurate NMO correction for primaries, this shows reverberation period as a function of offset and arrival time. Bold lines show changes in period with arrival time along one ODR partial stack.

been substantially eliminated but the improvement in tie of primaries on the partial stack data is not outstanding.

Reverberations

Autocorrelograms of the spliced partial stacks at each line intersection provide insight into the nature of periodic energy in OAI. Figure 8 shows normalized autocorrelogram splices along line 11. The water-layer reverberations are identified by their residual moveout of about 25 ms and time delay of 85 ms at near offset. In this figure, the degree of similarity of multiples is displayed across offset and time separately from the primary arrivals. Multiples often tie quite well in much of the prospect area. Long-period surface multiples have been suppressed by partial stacking and do not appear in this display. Periodicities with little or no moveout are presumably due to nonrandom geology and should be avoided when designing a deconvolution operator. As mentioned earlier, the deconvolution operator applied to our 4 ms data is 20 filter points long with a 60 ms gap and is indicated by the small vertical bar at left in the figure.

Figure 9 shows predicted residual normal moveout (RNMO), after correction with our global velocity model, for reverberations from a water layer with 85 ms two-way travelt ime and an interval velocity of 1500 m/s. The moveout

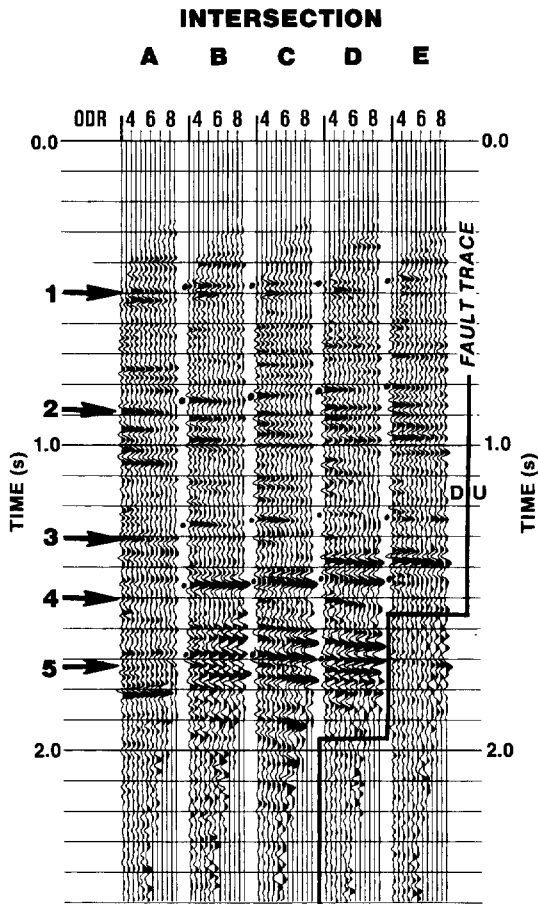


FIG. 10. ODR spliced partial stacks along dip line 11 deconvolved after stack. Arrows indicate interpreted events at intersection A, dots mark these at other intersections. The major fault is indicated by the solid line at the right.

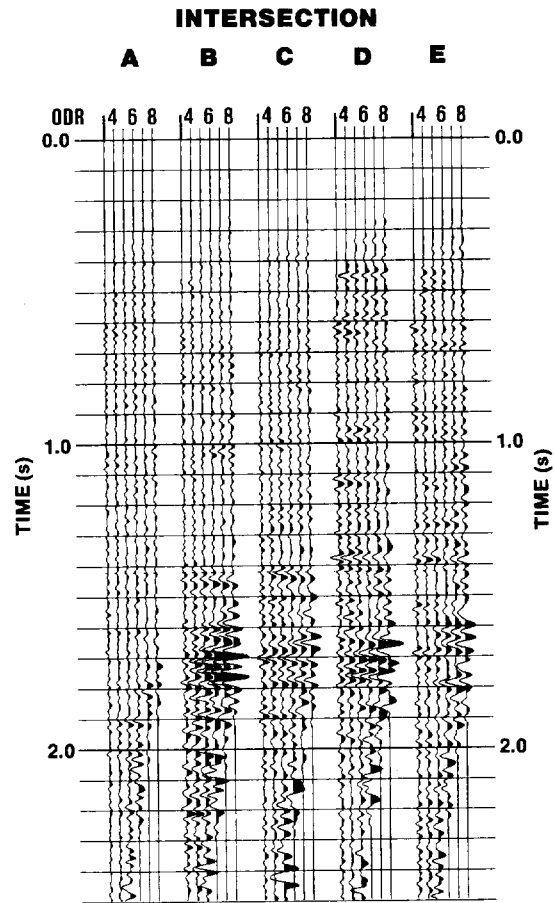


FIG. 11. Difference records formed by subtracting the strike traces from the dip traces of Figure 10. There is no amplification with respect to the input.

observed on autocorrelograms agrees well with this simple method. The bold lines connect offsets corresponding to constant ODR range, where those ODRs are full fold, i.e., are unaffected by the mute pattern. The light lines show the predicted moveout for reverberations on an NMO corrected CMP gather. Variations in arrival time across offset indicate changes in reverberation period with respect to the applied velocity function. Clearly, reverberation period changes with time along an ODR trace; however, in practice, a single design and application gate is suitable at the current level of processing. The deconvolution operator, which was designed over one gate after divergence correction, is a biased estimate of reverberation period. It is most effective on the strong reverberations in the target zone. Reverberations in other intervals are not estimated as well but are weaker and less noticeable.

A weak, second-bounce reverberation of positive polarity also matches calculated arrival times and is visible at intersection D at about 1.42 s on Figure 8. At most locations, the reverberation has been reduced substantially by partial stacking because it has about 14 ms of residual moveout within each partial-offset gather.

Magnitude and nature of mis-ties

Figure 10 shows spliced partial stacks for line intersections along line 11, after gapped deconvolution based on the Figure 8 autocorrelograms. Figure 11 shows the corresponding partial stack difference records. The most striking feature on these figures is the large arrival time mis-tie at intersections B and D in the 1.6 to 1.8 time zone. These major mis-ties are attributed to the variable transmission effects of the deep gas zones and are discussed in more detail below. Note that the autocorrelogram ties (Figure 8) are not affected by these deep primary mis-ties.

With the exception of the time mis-ties related to the deep transmission anomalies, the correspondence between dip and strike lines shown in Figure 10 is visually impressive. For the most part, the residual moveout and the amplitude versus offset are duplicated on dip and strike lines. Significant regions show residual down by 20 dB, requiring an arrival time match of 0.5 ms or better and an amplitude correspondence to within 10 percent.

Since the maximum dip on line 11 is only about 3 degrees, the theoretical mis-tie is less than 0.5 ms. Intersection A, beyond the edge of the large hydrocarbon reservoirs, ties well even though this intersection has the most dip of any studied. Dip-related problems, such as reflection-point smear and velocity perturbation, are not strong enough at these low dip angles to significantly affect the tie.

The results shown in Figures 10 and 11 are typical of the prospect as a whole. The residual error between dip and strike lines averages about -8 dB. At locations away from the major line intersection mis-ties, an accurate tie with well data may be attempted. The study of this data set suggests that a 20 dB correspondence between the actual data and data predicted from a subsurface model is a reasonable interpretation objective. Deep and shallow transmission-path velocity anomalies are the major phenomena that lie outside the capabilities of conventional processing and are required to approach a 20 dB accounting of the data.

Interpretive use of intersection displays

Figures 12 and 13 show zoom displays of spliced partial stacks from lines 11, 13, and 15. Recall that a single depth-dependent velocity function was used to process these data. At stratal level 3, there is little evidence of significant residual NMO, suggesting that a time map should have the same form as a depth map. In contrast, a significant lateral

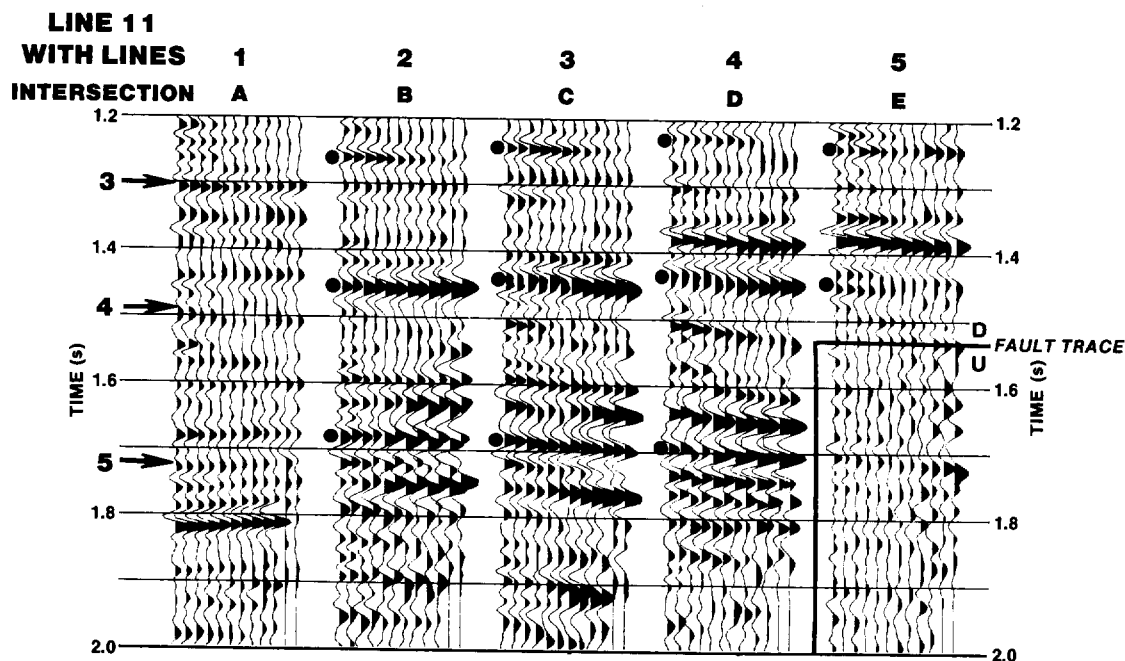


FIG. 12. Close up of the zone of largest mis-tie along line 11. The major fault trace is indicated at the right.

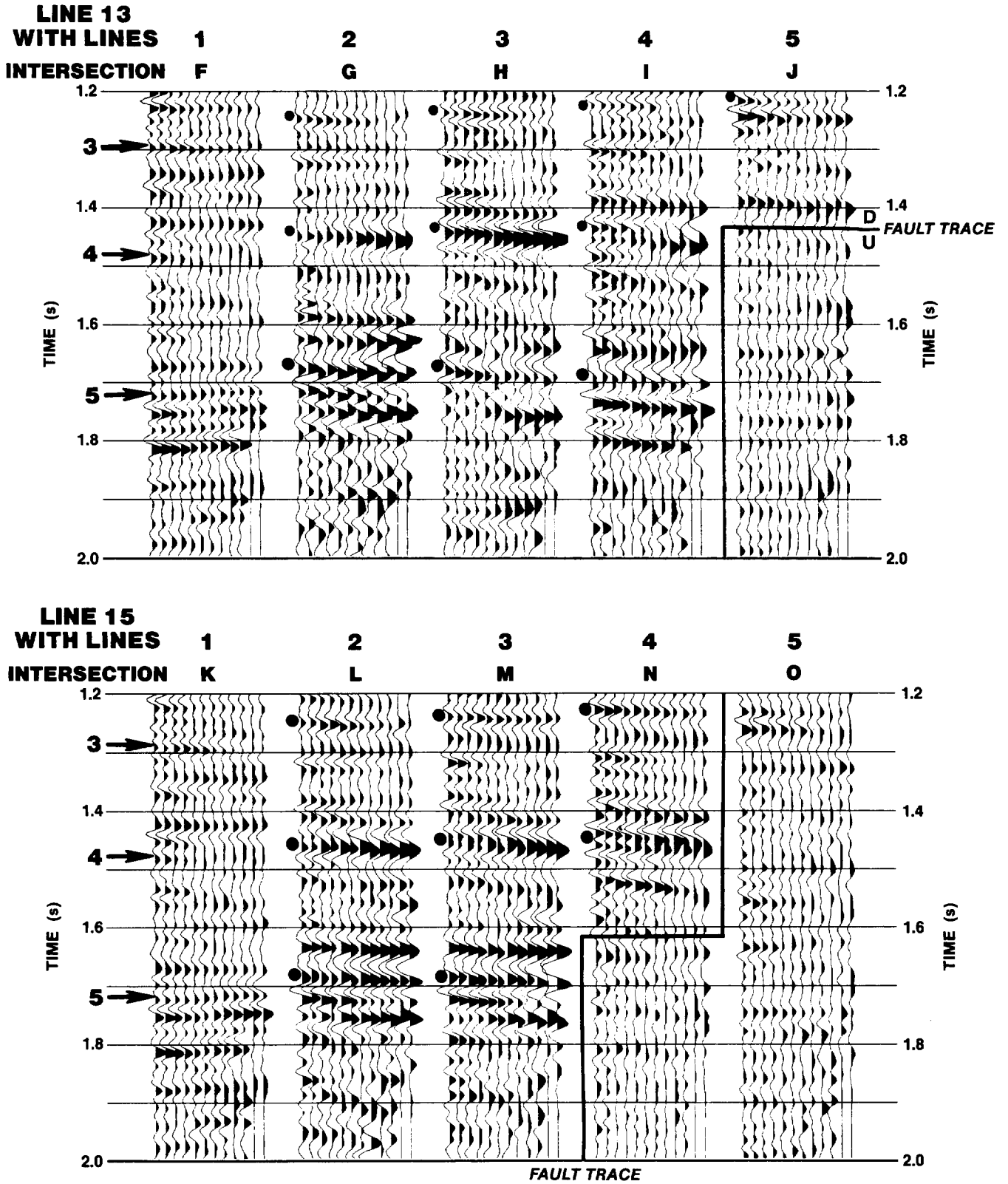


FIG. 13. Close up of the zone of largest mis-tie along lines 13 and 15. The major fault trace is indicated at the right.

variation in residual NMO is evident at stratal level 5. At the three intersections with line 1 (A, F, and K in Figure 1), the data at level 5 are overcorrected by 10–15 ms. At the three intersections with line 3 (C, H, and M), the data at level 5 are undercorrected by about 10 ms. We can directly translate 20 ms of residual NMO in these partial-stack displays to an equivalent of about 30 ms time-to-depth conversion perturbation. This 30 ms perturbation at a traveltime of 1.7 s corresponds roughly to a 1.8 percent change in rms velocity from line 1 to line 3 (which are separated by 1.5 km). Level 5 appears in the figures to be about 20 to 30 ms later on line 1 than on line 3. This implies that at line 1, level 5 is about 50 m downdip from line 3 if we use a laterally invariant velocity. However, the residual moveout suggests actual dip is about 100 m from line 3 to line 1.

Analysis of RNMO along the raypaths to the undercorrected events in Figure 12 indicates two low-velocity regions below 1.2 s near the crest of the structure on line 11. These intervals are associated with AVO anomalies and high amplitudes on the stack and correspond to deviations in interval velocity from the background function of approximately –7 percent and –9 percent. Transmission paths were determined by ray tracing through a model incorporating the perturbed interval velocities. This lateral velocity variation is consistent with the observed traveltime mis-ties observed at the intersections of the dip line with strike line 2. A corrected velocity model consistent with the mis-ties produces a depth section with much less rollover into the fault than is apparent on a depth section using the stacking velocities. Also, the structural crest is displaced from near strike line 2 toward the intersection of strike line 3. Detailed conventional velocity analyses near lines 1 and 3 give similar results. However, velocity analyses near lines 2 and 4 give unreasonable results, especially for small time intervals. Analysis of the line intersection mis-ties in the context of a two-dimensional earth explains this discrepancy.

Figure 14 shows the calculated RNMO across offset at selected arrival times for a perturbed interval velocity. These curves depict undercorrected arrivals at the specified

times on an NMO corrected CMP gather. The interpretation of RNMO as a linearized perturbation in velocity is discussed by Schneider and Backus (1968). The offsets corresponding to the middle of each ODR are marked with x's. An event at 1.6 s should exhibit about 13 ms of residual moveout between ODR 1 and ODR 8 if it is overlain by a 100 ms layer that is 20 percent slower than the applied NMO velocity. There is also a time delay at zero offset associated with a low-velocity layer. Therefore, we can calculate a factor to convert RNMO to changes in thickness. At 1.6 s, 13 ms of RNMO corresponds to a 20 ms reduction in time thickness for a 100 ms thick reference. The conversion factor for this velocity function is 20 divided by 13 or approximately 1.5. With such simple calculations and a laterally invariant velocity function, an interpreter can see at a glance the changes in thickness and interval velocity implied by the valid or tied RNMO along a line of ODR partial stacks.

An inspection of Figures 12 and 13 also illustrates the utility of the partial-stack line-intersection display in the interpretation of amplitude and amplitude-versus-offset anomalies. The general amplitude increase for the gas-bearing sand reservoirs updip, the reproducible decrease in amplitude versus offset at nonproductive level 3, the reproducible increase in amplitude with offset at productive level 4, and the constant amplitude versus offset at producing level 5 can all be considered reliable on the basis of the reproducibility exhibited in Figure 13. The observations show valid offset-dependent primary-reflection properties. The meaning of this valid primary-reflection offset dependence is another issue.

CONCLUSIONS

Deep and shallow velocity anomalies associated with hydrocarbons are the source of the largest mis-ties in the study area. The largest mis-ties on line 11 and some other lines in OA1 are caused by transmission through different amounts of gas encountered in the strike and dip directions at the edges of hydrocarbon reservoirs. Low velocities in the

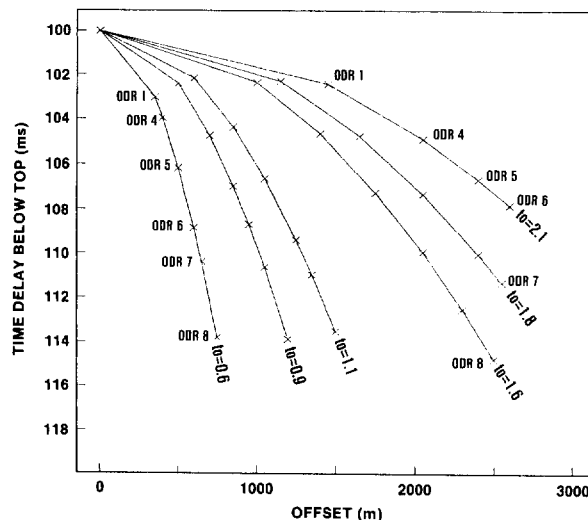


FIG. 14. Residual NMO as a function of offset and arrival time for events at the base of a 100 ms thick interval which is 20 percent slower than our applied NMO velocity.

gas zones produce a dynamic shift in arrival time and changes in amplitude.

Analysis of mis-ties in the offset dimension provides measurements of local deviations from one-dimensionality, as well as a quality control technique for data processing. Therefore, acquisition plans should provide for logical placement and an adequate number of intersections over potentially difficult or interesting structures. Techniques for exposing mis-ties include forming spliced gathers and difference records. Spliced gathers of angle-invariant partial stacks at line intersections summarize AVO, RNMO, and CMP mis-tie, i.e., validity of the 1-D assumption. A quick estimate of the degree of confidence to place in the seismic image can be obtained by examining a suite of difference panels of partial stacks over a prospect area. Also, autocorrelograms of the spliced partial stacks often expose significant multiple behavior. Line intersections should provide valuable information for detailed work such as AVO analysis, well-to-seismic ties, production and development studies, and inversion (Backus et al., 1987).

The OA1 marine data are of high quality and were recorded with simple, stable source and receiver arrays under good acquisition conditions. We have not addressed the challenge of complex geology and severe statics often encountered in land work or problems related to tying entirely different surveys. However, we expect prestack and partial-

stack line intersection mis-tie analysis to provide insight into these and other questions for both land and marine data.

ACKNOWLEDGMENTS

This study was supported by the sponsors of Project SEER. The data set was provided by Geophysical Service Incorporated.

REFERENCES

- Backus, M. M., and Chen, R. L., 1975, Flat spot exploration: *Geophys. Prosp.*, **23**, 533-577.
- Backus, M. M., Garcia, A. I., and Huston, D. C., 1987, On deconvolution and inversion in a one-dimensional earth, in Bernabini, M., Carrion, P., Jacovitti, G., Rocca, F., Treitel, S., Worthington, M., Eds., *Deconvolution and inversion*: Blackwell Scientific Publications, 208-225.
- Henry, M., and Mellman, G. R., 1988, Linearized simultaneous inversion for source wavelet equalization and mis-tie adjustment: 58th Ann. Internat. Mtg. Soc. Expl. Geophys., Expanded Abstracts, 953-955.
- Huston, D. C., 1987, Interpretation of seismic signal and noise through line intersection mis-tie analysis: M.A. thesis, Univ. of Texas at Austin.
- Newman, P., 1973, Divergence effects in a layered earth: *Geophysics*, **38**, 481-488.
- Schneider, W. A., and Backus, M. M., 1968, Dynamic correlation analysis: *Geophysics*, **33**, 105-126.
- Todd, C. P., and Backus, M. M., 1985, Offset dependent reflectivity in a structural context: 55th Ann. Internat. Mtg., Soc. Expl. Geophys., Expanded Abstracts, 586-588.
- White, R. E., 1984, Signal and noise estimation from seismic reflection data using spectral coherence methods: *Proc. IEEE*, **72**, 1340-1356.